

Elastic constants of bcc austenite and 2H orthorhombic martensite in CuAlNi shape memory alloy

P. Sedlák^{a,c}, H. Seiner^{a,c}, M. Landa^{a,*}, V. Novák^b, P. Šittner^b, Ll. Mañosa^d

^a Institute of Thermomechanics, The Academy of Sciences of the Czech Republic, Dolejškova 5, 182 00 Prague 8, Czech Republic

^b Institute of Physics, Czech Academy of Sciences, Na Slovance, 182 00 Prague 8, Czech Republic

^c CTU Faculty of Nuclear Sciences and Physical Engineering, Trojanova 13, 120 00 Prague 2, Czech Republic

^d Dept. d'Estructura i Constituents de la Materia, Facultat de Física, Universitat de Barcelona, Diagonal 647, Barcelona, Catalonia, Spain

Received 7 March 2005; received in revised form 6 April 2005; accepted 7 April 2005

Available online 3 June 2005

Abstract

Elastic constants of cubic austenite and orthorhombic 2H martensite phases in the Cu–Al–Ni shape memory alloy were determined by ultrasonic pulse-echo technique using multiple single crystal specimens and a novel optimization based evaluation method that minimizes the uncertainty stemming from experimental errors as well as experimental effort. Multiple martensitic single crystals were prepared from the austenite crystal by a dedicated deformation technique. Taking advantage of the fact that the elastic constants of the austenite and 2H martensite phase were evaluated on the same piece of material, soft acoustic modes and elastic properties of both phases were compared taking into account the lattice correspondence. It is found that the 2H martensite crystal partially inherits the soft acoustic modes of the austenite and hence its elastic properties.

© 2005 Acta Materialia Inc. Published by Elsevier Ltd. All rights reserved.

Keywords: Acoustic methods; Elastic behavior; Shape memory alloys; Martensitic phase transformation

1. Introduction

Shape memory alloys (SMA) exhibit unique thermo-mechanical behaviors due to thermoelastic martensitic transformations (MT) driven by the external stress or temperature [1–3]. It is of essential interest to know the elastic constants of the austenite and martensite phases, since they reflect the fundamental thermodynamic properties; i.e., very interesting physical information can be deduced not just from the values of elastic constants but mainly from their temperature and stress dependencies [3]. Knowledge of the elastic constants of both austenite and martensite phases is also important in modelling of SMA functional mechanical behaviors,

since the crystal domains (separated by mobile phase or twin interfaces responsible for shape memory phenomena) interact elastically.

Elastic properties of the cubic high temperature phases in SMAs are relatively well known [2–5], including their temperature [3–5] and stress [2,3] dependencies. As a particular case to be focused on in this work, the β_1 austenite phase in Cu-based SMAs is known for its very large elastic anisotropy. It transforms to various martensitic phases β'_1 (18R), γ'_1 (2H), α'_1 (6R) depending on composition, temperature, magnitude and sense of uniaxial stress [1]. Before the martensitic transformation occurs at M_s temperature, the body-centered cubic (bcc) structure of the austenite [4] exhibits several kinds of anomalies (elastic, diffraction, phonon) over a broad temperature range above M_s . These anomalies can be viewed as a reflection of the enhanced instability of the bcc structure approaching its stability limit. In particular, variation of the elastic

* Corresponding author. Tel.: +420 2 605 3672; fax: +420 2 8658 4695.

E-mail address: ml@it.cas.cz (M. Landa).

constants of the β_1 austenite phase with temperature in the vicinity of the phase transition has been thoroughly investigated [3–5]. It is now generally accepted that the main characteristic feature of the pretransformation elastic instability of Cu-based SMAs is the simultaneous decrease of the elastic constant C' (softening) and increase of the C_{44} constant (hardening) with decreasing temperature. The experimental results published so far [3,4], however, prove that the softening is far from complete and that C' remains finite even just above M_s and the same is true for the softening of the [1 1 0] TA_1 phonon branch as another premartensitic instability observed in inelastic neutron scattering experiments [3].

There exist only very limited experimental data for the elastic properties of the low temperature (high stress) martensite phases in SMAs. This is mainly because of the experimental difficulties related to the preparation of multiple, sufficiently large single crystals of low symmetry martensite phases needed for the ultrasonic experimental methods commonly used to evaluate the elastic constants. Nevertheless, as regards the elastic properties of the lower symmetry martensite phases in Cu-based SMAs, some very limited data exist. Elastic constants of the 2H martensite phase in CuAlNi alloy were determined solely by Yasunaga et al. [8] using resonant ultrasound spectroscopy (RUS) technique. These constants, although never verified, as far as we know, are frequently referenced in the literature and widely used in SMA modelling. Elastic constants of the 18R monoclinic martensite in a different CuZnAl alloy were reported by Rodríguez et al. [7] and their temperature dependence investigated by González-Comas et al. [6]. In the present work, elastic constants of the bcc austenite (β_1) and orthorhombic 2H martensite phase (γ'_1) in CuAlNi single crystal were evaluated using an optimization

approach towards pulse-echo overlapping acoustic method. This newly proposed modification of the standard direct method (Section 2.3) is particularly suitable for evaluation of elastic constants of low symmetry martensite phases in SMAs. It facilitates the work and reduces experimental errors.

A deformation technique allowing the mutually conversion of the austenite and martensite single crystal variants (Section 3.2) was developed. The elastic constants of both austenite and martensite phases thus could be firstly evaluated on the same single crystal piece at the same temperature. Taking advantage of that, the inheritance of soft acoustic modes from bcc β_1 austenite to orthorhombic 2H martensite phase is investigated in Section 4.3. The inheritance of elastic properties (anisotropy of Young's modulus) is discussed in Section 4.4 as a model example for elastic property changes associated with the martensitic transformation in SMAs.

2. Experimental methods

2.1. CuAlNi single crystal

A single crystal of Cu–14.3Al–4.2%Ni (wt.%) alloy was grown by the Bridgman method. The transformation temperatures were determined by DSC as $M_s(2H) = 288$ K and austenite start temperature, $A_s = 313$ K. Due to the thermal hysteresis, this crystal may exist at room temperature either in the bcc austenite or in the 2H martensite phase. Four specimens (Table 1) were spark cut in the austenite phase in a prism shape (Table 2) with crystallographic orientations of the faces given in Table 1. The crystal lattice orientations were determined by back-reflection Laue method with an accuracy better than 2° .

Table 1
Orientations of the CuAlNi single crystal specimens in austenite state

Samples	Face A			Face B			Face C		
Sample 1	0.577	0.577	0.577	−0.816	0.408	0.408	0	0.5	−0.5
Sample 2	0.988	−0.122	0.087	−0.105	−0.052	0.993	−0.140	−0.980	−0.070
Sample 3	−0.018	0.070	0.997	0.809	0.588	0.000	−0.585	0.806	−0.087
Sample 4	0.601	−0.799	−0.052	0.669	0.454	0.616	0.438	0.407	−0.788

Samples 1–3 – cube (5.6 mm), sample 4 – prism ($a = 6.592$ mm, $b = 5.561$, $c = 5.945$).

Table 2
Shape changes of sample 4 during compression tests (Figs. 2 and 4)

Sample	a (mm)		b (mm)		c (mm)		α		β		γ	
Austenite	6.592		5.561		5.945		91.665		90.935		89.85	
Martensite	exp.	cal.	exp.	cal.	exp.	cal.	exp.	cal.	exp.	cal.	exp.	cal.
Variant 6	6.96	6.993	5.487	5.487	5.692	5.693	86.19	86.11	91.36	92.52	88.59	88.42
Variant 5	6.748	6.748	5.548	5.619	5.592	5.784	84.37	84.11	91.55	93.06	89.43	89.56
Variant 4	6.348	6.37	5.642	5.578	6.103	6.162	94.13	94.01	86.93	86.44	84.01	85

The thicknesses a , b , c and angles α , β , γ are measured on martensite parallelepipeds as suggested in Fig. 3(b).

The mass density $\rho = (7.055 \pm 0.064) \times 10^3 \text{ kg m}^{-3}$ was evaluated by the Archimedes technique.

2.2. Ultrasonic pulse-echo method

Elastic constants were evaluated by ultrasonic pulse-echo method [9]. Velocities of propagation of quasi-longitudinal (qL) and quasi-transverse (qT) acoustic waves were measured in general crystal directions. The preposition quasi refers to the fact that the acoustic waves propagating along a general crystal direction of the anisotropic solid are not pure longitudinal and pure transversal but can be divided in one nearly longitudinal wave qL with small shear component and two nearly transversal waves qT1 and qT2 with small longitudinal component.

Two sets of delayed broadband transducers for generation and receiving acoustic waves (10 or 30 MHz for qL waves and 5 or 20 MHz for qT-waves) were used with a pulse/receiver system DPR50+ (JSR Ultrasonics). Honey was used for acoustic coupling between transducer and specimen for transverse waves and propylene glycol for longitudinal waves. The time of flight measurement was carried out by pulse overlapping technique implemented in a digital storage oscilloscope LT264M (LeCroy). Results obtained by the two different frequency bands measurements were compared and the influence of wave dispersion to velocity measurements was evaluated. It was found that the dispersion effect contributed much less to the uncertainty in measured elastic constants than other experimental errors and was therefore neglected.

2.3. Procedure for evaluation of the elastic constants

In order to precisely evaluate the elastic constants of elastically anisotropic materials (as, for example, the CuAlNi studied in this work) by the traditional pulse-echo ultrasonic method, single crystal samples have to be cut along the specific crystal directions with a very high precision. Velocities of longitudinal and transverse acoustic waves $v[mnu][pqr]$ propagating in $[mnu]$ crystal directions with wave polarization in $[pqr]$ direction are measured. For cubic crystals, three independent elastic constants C_{11} , C_{12} , C_{44} may be conveniently evaluated from the acoustic velocities (direct traditional method) measured in $[100]$ (Eqs. (1a) and (1b)) and $[110]$ (Eqs. (2a)–(2c)) crystal directions.

$$v_{11} = v_{[001][001]} = \sqrt{\frac{C_{11}}{\rho}}, \quad (1a)$$

$$v_{44} = v_{001\text{plane}} = \sqrt{\frac{C_{44}}{\rho}}, \quad (1b)$$

$$v_{qL} = v_{[110][110]} = \sqrt{\frac{C_{11} + C_{12} + 2C_{44}}{2\rho}}, \quad (2a)$$

$$v_{C'} = v_{[110][1-10]} = \sqrt{\frac{C'}{\rho}}, \quad (2b)$$

$$v_{C_{44}} = v_{[110][001]} = \sqrt{\frac{C_{44}}{\rho}}, \quad (2c)$$

where ρ is the mass density. In case of cubic materials, the elastic constant C_{44} is associated with the pure shears in the (001) basal plane and the elastic constant C' (Eq. (3)) with pure shears $[110][1-10]$.

$$C' = (C_{11} - C_{12})/2. \quad (3)$$

In order to characterize the elastic anisotropy of cubic materials, factor A (Eq. (4)) is commonly expressed as a ratio of these elastic constants:

$$A = C_{44}/C'. \quad (4)$$

Since C_{44} is large and C' is low for bcc materials, the anisotropy factor for bcc is $A > 1$ and reaches values as large as $A \sim 13$ for strongly anisotropic materials such as CuAlNi [3,4].

In the case of lower symmetry structures, more measurements on multiple samples have to be carried out to evaluate all independent elastic constants. Specific equations for wave velocity calculation in some symmetric directions of the orthorhombic structure (similar to Eqs. (1)–(2)) can be found in [9]. Since this is rather laborious and there are difficulties with preparation of detwinned martensite single crystals, the elastic constants of many low symmetry martensite phases in SMAs are not known yet. However, even the evaluation of elastic constants of the austenite phase by the pulse-echo method becomes problematic in the case of strongly elastically anisotropic solids. In such cases, certain measured acoustic wave velocities $v_{[mnu][pqr]}$ depend strongly on the precision in determination of $[mnu]$ and $[pqr]$ directions. Any experimental error in specimen orientation may significantly lower the precision of the corresponding elastic constants and thus decrease the overall data quality. The difficulties described above lead us to develop a modified approach (alternative to the traditional direct method) applicable to the evaluation of elastic constants of both austenite and martensite phases facilitating the work. Taking advantage of the possibility to prepare a large number of samples with different crystallographic orientations (Table 1, Section 3.2), a weighted optimization procedure (Fig. 1) was developed to minimize the effect of experimental errors in the evaluation of elastic constants C_{IJ} .

In a general anisotropic solid, one quasi-longitudinal qL and two quasi-transverse acoustic waves qT1 and qT2 propagate in a given direction with mutually

1. Inputs from the measurements : Velocities v_p^{exp} in directions $\mathbf{n}^{(p)}$ for $p = 1, \dots, N$ and the mass density ρ
2. Preliminary determination of elastic constants : C_{IJ}^0 as a result of the optimization procedure :

$$Q = \sum_{p=1}^N [v_p^{\text{exp}} - v^{\text{cal}}(C_{IJ}^0, \mathbf{n}^{(p)})]^2 \rightarrow \min$$

where the function $v^{\text{cal}}(C_{IJ}, \mathbf{n}) : \det(\Gamma_{ik} - \rho v^2 \delta_{ik}) = 0$

3. Determination of the set of directions $\mathbf{n}^{(p,m)}$ distributed around $\mathbf{n}^{(p)}$ for the random variable $\vartheta = \cos^{-1}(\mathbf{n}^{(p)} \cdot \mathbf{n}^{(p,m)})$ with chosen $\sigma_\vartheta = 2^\circ$ and mass density values $\rho^{(m)} \in (0.9\rho; 1.1\rho)$ simultaneously for $m = 1, \dots, M$, ($M = 30$)
4. Weight calculation : $w_p = [\text{sdev}(v_p^{(m)})]^{-1}$, where the velocity set is $v_p^{(m)} = v^{\text{cal}}(C_{IJ}^0, \mathbf{n}^{(p,m)})$
5. Determination of C_{IJ} as a result of the optimization procedure :

$$Q = \sum_{p=1}^N w_p^2 [v_p^{\text{exp}} - v^{\text{cal}}(C_{IJ}, \mathbf{n}^{(p)})]^2 \rightarrow \min$$

6. If $|C_{IJ} - C_{IJ}^0| < \text{error}$, then $C_{IJ} \rightarrow C_{IJ}^{\text{Opt}}$, else $C_{IJ} \rightarrow C_{IJ}^0$, goto 3

Fig. 1. Flowchart of the weighted optimization method used for the evaluation of elastic constants.

perpendicular polarization vectors. In the modified approach, the propagation velocities v^{exp} of longitudinal wave qL and fast (qT1) and slow (qT2) transverse acoustic waves were measured in multiple austenite and martensite crystal directions \mathbf{n} (Tables 3 and 6) without specifying the wave polarization vectors. An error function $Q(C_{IJ})$ in phase velocities was introduced and minimized with respect to all independent elastic constants C_{IJ} ($I, J = 1, 2, \dots, 6$) as

$$Q = \sum_{p=1}^N w_p^2 \cdot (v^{\text{exp}}(\mathbf{n}^{(p)}) - v^{\text{cal}}(C_{IJ}^{\text{Opt}}, \mathbf{n}^{(p)}))^2 \rightarrow \min, \quad (5)$$

where $\mathbf{n}^{(p)}$ is a unit vector in the direction of propagation of the p th input (measured) phase velocity, N is the number of phase velocities used in the procedure and “Opt” denotes the resulting values of C_{IJ} obtained by the iterative procedure described in Fig. 1 and w is the weight vector discussed below. The calculated phase velocities

Table 3
Velocities of propagation of qL and qT1 acoustic waves in CuAlNi austenite phase

Propagation direction \mathbf{n} (direction cosines)			Wave velocity [10^3 m/s]			
			qL		qT1	
x	y	z	exp.	cal.	exp.	cal.
0.577	0.5771	0.577	6.032 ± 0.022	6.036	–	–
0	0.5	0.5	5.679 ± 0.025	5.690	3.662 ± 0.042	3.674
–0.816	0.408	0.408	5.735 ± 0.157	5.792	–	–
0.988	–0.122	0.087	4.841 ± 0.266	4.744	3.621 ± 0.055	3.641
–0.105	–0.052	0.993	4.637 ± 0.243	4.660	3.664 ± 0.039	3.660
–0.140	–0.980	–0.070	4.831 ± 0.266	4.760	–	–
–0.018	0.070	0.997	4.452 ± 0.207	4.564	3.668 ± 0.023	3.672
0.809	0.588	0.000	5.641 ± 0.094	5.626	3.650 ± 0.043	3.674
–0.585	0.0806	–0.087	5.678 ± 0.106	5.648	3.675 ± 0.120	3.629

exp. – Experimentally measured values; cal. – values calculated inversely from refined elastic constants.

$v^{\text{cal}}(C_{IJ}, \mathbf{n}^{(p)})$ were obtained as solutions of the eigenvalue problem [10], which can be written in the tensor form ($i, j, k, l = 1, 2, 3$) as

$$\det |\Gamma_{ik} - \rho v^2 \delta_{ik}| = 0, \quad (6)$$

$$\Gamma_{ik} = n_j C_{ijkl} n_l, \quad (7)$$

where Γ_{ik} is the Christoffel's matrix for the chosen direction \mathbf{n} and for the elastic tensor C_{ijkl} , δ_{ik} is the Kronecker's symbol. The general solutions of Eq. (6) are three real positive eigenvalues giving wave velocities and corresponding eigenvectors (wave polarization). Thus, the solution for given direction \mathbf{n} represents propagation of three planar acoustic waves with phase velocities ($q_L > q_{T1} \geq q_{T2}$) and mutually perpendicular polarization vectors. The global minimum of the error function $Q(C_{IJ})$ was found by a simplex method.

When developing the weighted optimization procedure we were inspired by the "self-consistent procedure" proposed by Rodríguez et al. [7] while evaluating the elastic constants of monoclinic 18R martensite. The main advantage of the weighted optimization procedure over the standard evaluation method is that it leads to minimization of the uncertainty in evaluated elastic constants stemming from the inaccuracy in the determination of the exact crystal orientation. These errors are even larger than the experimental errors directly related to the time of flight measurements. Moreover, in the case of measurements made in general crystal directions, we do not have to specify the polarization direction vectors. The first step of the weighted optimization procedure is the calculation of elastic constants from the measured wave velocities all having the same weight. Next, standard deviations σ_v of the wave velocities v are determined by Monte Carlo simulation using the starting guess of elastic constants C_{IJ}^0 . Random vectors of the wave propagation are generated with Gaussian distribution (given by standard deviation σ_φ estimated as 2°) around the directions perpendicular to the sample faces evaluated by the Laue method. The reciprocal values of obtained standard deviations σ_v are taken as the weights w in the final optimization generating the elastic constants, i.e.,

$$w(C_{IJ}^0, \mathbf{n}) = \sigma_v^{-1}. \quad (8)$$

If there appears a considerable difference in the values of elastic constant, a new calculation is performed until the elastic constants remain stable.

3. Experimental results

3.1. Elastic constants of the austenite phase

The pulse-echo measurements were performed at room temperature $T = 296$ K on three austenite cubes in nine available crystal directions (Table 1). The measured and calculated wave velocities for longitudinal and transverse waves are given in Table 3. The denoted error intervals stem from the orientation uncertainty. They were determined by the Monte Carlo simulation approach introduced above. Some data are missing in the table because only a weak echo could be detected in some ultrasound propagation modes due to the differences in the directions of phase and group velocities (related energy flux) of acoustic waves propagating in general directions of strongly anisotropic CuAlNi crystals. The obtained elastic constants of the austenite phase are given in Table 4. The denoted experimental errors of the elastic constants were determined considering inputs varying in the error range $\pm 1\%$ of the mass density and the confidence intervals of phase velocities from Table 3. The high inaccuracy of the coefficient of elastic anisotropy A is mainly due to the error in the evaluation of the C' constant. More accurate measurement of the anisotropy coefficient A can be performed by the RUS technique where resonances corresponding to low valued elastic constants C' are easily and precisely determined. An increase in anisotropy factor from $A \sim 11.6$ at room temperature down to $A \sim 12.8$ at M_s (175 K) was reported in our earlier work [13] on a similar CuAlNi single crystal. The present work elastic constants of CuAlNi austenite are compared in Table 4 with a few selected literature data.

3.2. Elastic constants of the 2H martensite phase

The CuAlNi austenite transforms into the orthorhombic 2H martensite upon cooling below the martensite start temperature $M_s = 288$ K and, due to thermal hysteresis, remains in this phase upon heating up to

Table 4

Elastic constants of the cubic austenite phase in CuAlNi measured in this work and comparison with selected literature data

Source	Alloy composition	C_{11} (GPa)	C_{12} (GPa)	C_{44} (GPa)	$A = 2C_{44}/(C_{11} - C_{12})$	$C' = (C_{11} - C_{12})/2$ (GPa)
This work	Cu–14.3wt.%Al–4.2wt.%Ni	142.38 \pm 0.70	124.10 \pm 2.06	95.24 \pm 0.42	10.42 \pm 1.24	9.14 \pm 1.09
[11]	Cu _{2.726} Al _{1.122} Ni _{0.152}	142.5	127.5	95.0	12.9	7.35
[11]	Cu _{2.742} Al _{1.105} Ni _{0.152}	137.0	122.7	95.0	13.3	7.15
[2]	Cu–14.3wt.%Al–4.1wt.%Ni	142.8	126.8	95.9	12.0	8.00
[12]	Cu–14wt.%Al–4.1wt.%Ni	143.1	124.3	94.1	10.0	9.4

room temperature. Taking advantage of this, samples for measurement of elastic constants of 2H martensite phase were prepared from the austenite samples used earlier to evaluate the austenite elastic constants. Both measurements were carried out at room temperature. However, the martensite phase forms upon cooling in a self-accommodating manner with many internal twin interfaces between and within the individual variants so that a single crystal of the martensite phase is not obtained by simple cooling. A single detwinned variant of the 2H martensite phase, however, can still be obtained by applying a suitable sequence of uniaxial compression loads to the originally cube (prism) shaped austenite crystal. Following the first compression load, the original prismatic shape is lost and the sample attains the shape of a parallelepiped. Upon successive compression loads on the three different faces of the martensite parallelepiped, the shape of the martensite crystal changes among various parallelepipeds corresponding to certain variants of the 2H martensite phase. Any martensite parallelepiped can be transformed back to the original austenite prism specimen by heating above $T = 353$ K (as a result of the deformation in the 2H martensite state [1,2], the austenite finish temperature, A_f , is shifted ~ 40 K upwards).

The crystallographic data of the phases (austenite bcc: $a_0 = 0.5835$ nm, martensite orthorhombic 2H: $a = 0.4389$ nm, $b = 0.5342$ nm, $c = 0.4224$ nm) were taken from the literature [15]. The coordinate system x , y , z in the martensite phase has been selected as shown in Fig. 2(a) (i.e., $x \parallel [1\ 0\ 0] \sim a$, $y \parallel [0\ 1\ 0] \sim b$, $z \parallel [0\ 0\ 1] \sim c$). The relation between the directions and planes of austenite and 2H martensite phases in CuAlNi is given by the characteristic lattice correspondence. Six lattice correspondence variants of the 2H martensite phase are described by the transformation matrices given in

Table 5. Fig. 2 shows the orientation relationship for the variant 1. Let us remind that the transformation matrices would be different for another martensite coordinate system (with respect to a , b and c lattice parameters) sometimes used in the literature. Relations between the Miller indexes of lattice correspondent crystal planes ($h\ k\ l$) and crystal directions $[t\ u\ v]$ in both phases are given by the transformation equations (9) and (10):

$$(h\ k\ l)_M^T = \mathbf{P}_i \cdot (h\ k\ l)_A^T, \quad (9)$$

$$[t\ u\ v]_M^T = \mathbf{D}_i \cdot [t\ u\ v]_A^T, \quad (10)$$

where \mathbf{P} and \mathbf{D} are transformation matrices for planes and directions, respectively (Table 5). The indexes M, A and i refer to martensite, austenite and martensite variant, respectively, superscript T denotes transpose. The transformation stretch matrices \mathbf{F} (Table 5) for individual variants were calculated from the lattice parameters of the bcc and 2H structures. The matrices \mathbf{F} enable the calculation of dimensional changes associated with the martensitic transformation and with the reorientation between two distinct martensite variants i .

An example for the compression deformation procedure will be illustrated for sample 4. The compression stress–strain curves are shown in Fig. 3(a), the sample shapes in Fig. 4 and geometrical data of individual martensite variant parallelepiped shapes (a , b , c , α , β , γ introduced in Fig. 3(b)) are given in Table 2. Sample 4 was three times deformed in the austenite state by applying compression on faces A–C. Very different σ – ε responses were recorded (AM-A, AM-B, AM-C in Fig. 3(a)). After the last compression on face C, the sample existed in the parallelepiped shape corresponding to the variant 6 (Fig. 4, Table 2). The specimen was next deformed again in the martensite state by applying compression load on face A (σ – ε curve MM-AC in Fig. 3(a)). During the deformation, the sample changed its shape at first into variant 5 (end of the 1st plateau) and then into variant 4 (end of the 2nd plateau). The two stress plateaus on the σ – ε curve MM-AC (Fig. 3(a)) correspond to two different twinning processes in the 2H martensite phase. Two sets of differently oriented traces of moving twin interfaces were clearly recognized on the sample faces by the optical microscope attached to the stress rig.

The martensite parallelepiped single crystals for acoustic measurements (Table 6) were prepared by dedicated sequences of compression loads applied subsequently on different sample faces. In order to minimize the experimental error in martensite elastic constants, it is essential that the martensite parallelepipeds used in ultrasonic measurements are true martensite single crystals with no internal interfaces. This is rather difficult to achieve and must be carefully examined. To check whether the prepared parallelepiped shapes indeed

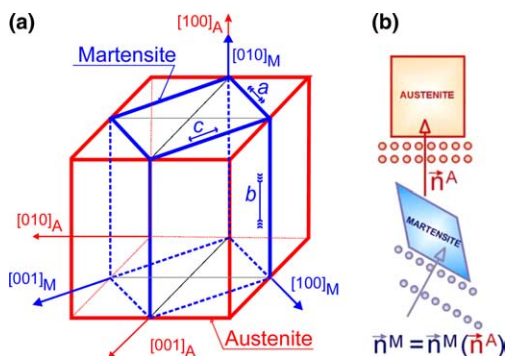


Fig. 2. Lattice correspondence (a) between the bcc austenite ($a_0 = 0.5835$ nm) and variant 1 of the 2H orthorhombic martensite phase ($a = 0.4389$ nm, $b = 0.5342$ nm, $c = 0.4224$ nm). The arrows suggest the magnitude and sense of transformation strains 6.37%, -8.46% and 2.37% along three basic directions of the 2H martensite structure, respectively. Lattice correspondent atomic planes in the austenite and martensite phases have generally different lattice spacing (b) and are not necessarily exactly parallel each other.

Table 5

Lattice correspondence (**D**, **P**) and transformation stretch (**F**) between the cubic austenite and orthorhombic 2H martensite in CuAlNi ($E_b = 0.91542$, $E_d = 1.04370$, $E_s = 0.02002$; lattice parameters – austenite: $a_0 = 0.5835$ nm; 2H martensite: $a = 0.4389$ nm, $b = 0.5342$ nm, $c = 0.4224$ nm)

Variant	Transformation matrix		Transformation stretch matrix, F , A → M
	D , A → M – directions	P , A → M – planes	
1	$\begin{pmatrix} 0 & -1 & 1 \\ 1 & 0 & 0 \\ 0 & 1 & 1 \end{pmatrix}$	$\begin{pmatrix} 0 & -1/2 & 1/2 \\ 1 & 0 & 0 \\ 0 & 1/2 & 1/2 \end{pmatrix}$	$\begin{pmatrix} E_b & 0 & 0 \\ 0 & E_d & -E_s \\ 0 & -E_s & E_d \end{pmatrix}$
2	$\begin{pmatrix} 0 & 1 & 1 \\ 1 & 0 & 0 \\ 0 & 1 & -1 \end{pmatrix}$	$\begin{pmatrix} 0 & 1/2 & 1/2 \\ 1 & 0 & 0 \\ 0 & 1/2 & -1/2 \end{pmatrix}$	$\begin{pmatrix} E_b & 0 & 0 \\ 0 & E_d & E_s \\ 0 & E_s & E_d \end{pmatrix}$
3	$\begin{pmatrix} 1 & 0 & -1 \\ 0 & 1 & 0 \\ 1 & 0 & 1 \end{pmatrix}$	$\begin{pmatrix} 1/2 & 0 & -1/2 \\ 0 & 1 & 0 \\ 1/2 & 0 & 1/2 \end{pmatrix}$	$\begin{pmatrix} E_d & 0 & -E_s \\ 0 & E_b & 0 \\ -E_s & 0 & E_d \end{pmatrix}$
4	$\begin{pmatrix} 1 & 0 & 1 \\ 0 & 1 & 0 \\ -1 & 0 & 1 \end{pmatrix}$	$\begin{pmatrix} 1/2 & 0 & 1/2 \\ 0 & 1 & 0 \\ -1/2 & 0 & 1/2 \end{pmatrix}$	$\begin{pmatrix} E_d & 0 & E_s \\ 0 & E_b & 0 \\ E_s & 0 & E_d \end{pmatrix}$
5	$\begin{pmatrix} -1 & 1 & 0 \\ 0 & 0 & 1 \\ 1 & 1 & 0 \end{pmatrix}$	$\begin{pmatrix} -1/2 & 1/2 & 0 \\ 0 & 0 & 1 \\ 1/2 & 1/2 & 0 \end{pmatrix}$	$\begin{pmatrix} E_d & -E_s & 0 \\ -E_s & E_d & 0 \\ 0 & 0 & E_b \end{pmatrix}$
6	$\begin{pmatrix} 1 & 1 & 0 \\ 0 & 0 & 1 \\ 1 & -1 & 0 \end{pmatrix}$	$\begin{pmatrix} 1/2 & 1/2 & 0 \\ 0 & 0 & 1 \\ 1/2 & -1/2 & 0 \end{pmatrix}$	$\begin{pmatrix} E_d & E_s & 0 \\ E_s & E_d & 0 \\ 0 & 0 & E_b \end{pmatrix}$

correspond to fully detwinned martensite variants, their geometrical characteristics $a, b, c, \alpha, \beta, \gamma$ (Fig. 3(b)) were compared with theoretically calculated values corre-

sponding to the required martensite variant. Table 2 shows results of such comparison for sample 4 used in deformation tests described in Figs. 3 and 4. As an additional check, the polished faces A–C of the samples were inspected for traces of twinning interfaces. Martensite variant single crystals exhibiting satisfactory agreement between experimental and calculated shapes typically shown faces with no interface traces. It was empirically found that good martensite variant single crystals were only prepared by applying compression load sequences suitable for each particular sample. For example, good single crystal of the 1st 2H martensite variant (Table 5) was obtained through a sequence of four compression loadings on parallelepiped faces of sample 1 in a sequence (B → C → A → B).

Multiple martensite parallelepipeds with different face orientations were prepared from three differently oriented austenite cubes (samples 1–3 in Table 1) for the pulse-echo ultrasonic measurements using the above outlined procedure. The measurements were carried out for 15 propagation directions of one quasi-longitudinal (qL) and two quasi-transverse acoustic waves (qT1, qT2). The experimentally measured wave velocities (exp.) are given in Table 6. The elastic constants of the

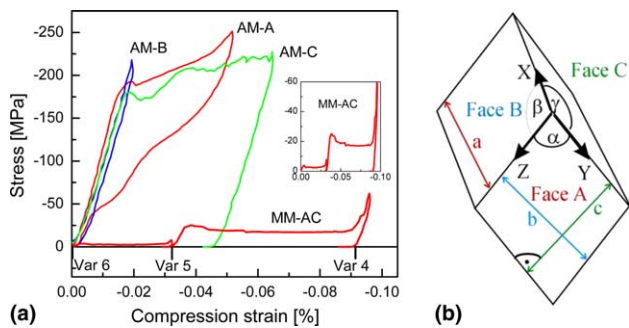


Fig. 3. (a) Stress–strain curves of sample 4 during compression tests at $T = 296$ K. The curves denoted as AM-A, AM-B, AM-C correspond to stress-induced transformation during compression loads on different faces A–C in austenite state. The two-stage curve MM-AC corresponds to martensite twinning during compression load on face A starting from the parallelepiped obtained before by previous full compression on face C. (b) Orthogonal coordinate system XYZ of sample 4 (aligned with sample edges in the austenite prism shape) and geometrical parameters ($a, b, c, \alpha, \beta, \gamma$) used to characterize the martensite parallelepiped shapes (Table 2, Fig. 4).

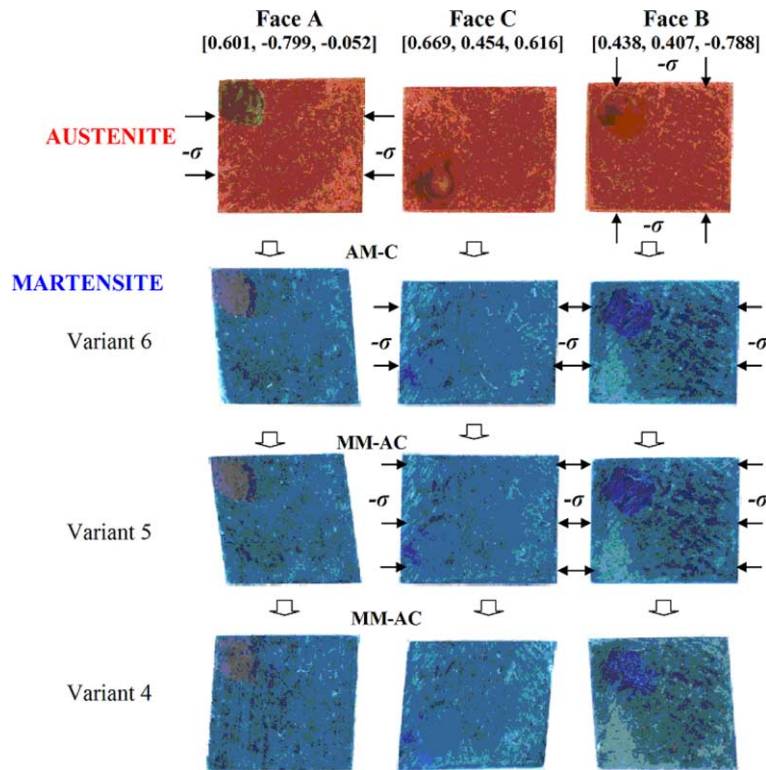


Fig. 4. Shape changes of the sample 4 in three subsequent mechanical tests (rows, Fig. 3(a)) documented by macroscopic views of three sample faces (columns). The photos demonstrate the large shape changes associated with transformation to individual martensite variants in subsequent compression tests: (1) compression on face C from the austenite state to variant 6 (AM-C curve in Fig. 3); (2) followed by compressive deformation on face A from variant 6 to variant 5 (MM-AC curve in Fig. 3 – end of 1st plateau) and (3) further compression to variant 4 (MM-AC curve in Fig. 3 – end of 2nd plateau). See also Table 2.

Table 6

Velocities of propagation of qL, qT1 and qT2 acoustic waves in 2H martensite phase in CuAlNi

Propagation direction \mathbf{n} (direction cosines)			Wave velocity (10^3 m/s)					
			qL wave		qT1 wave		qT2 wave	
x (a)	y (b)	z (c)	exp.	cal.	exp.	cal.	exp.	cal.
0	-0.8452	0.5344	5.176 ± 0.141	5.201	–	–	–	–
-1	0	0	5.111 ± 0.020	5.113	2.926 ± 0.040	2.930	1.803 ± 0.050	1.8000
0	0.6203	0.7844	5.602 ± 0.094	5.569	2.707 ± 0.069	2.732	2.245 ± 0.127	2.301
0.7726	0.6348	0	5.543 ± 0.019	5.536	2.343 ± 0.145	2.393	–	–
0.5198	-0.8543	0	5.318 ± 0.127	5.340	2.789 ± 0.110	2.782	–	–
0	0	1	5.770 ± 0.017	5.815	3.048 ± 0.010	3.068	1.803 ± 0.039	1.800
0.4574	0.7516	-0.4753	5.354 ± 0.049	5.296	3.177 ± 0.065	3.166	1.660 ± 0.184	1.632
-0.8392	0.4597	-0.2907	5.300 ± 0.112	5.356	–	–	–	–
-0.273	0.4486	0.851	5.551 ± 0.107	5.572	–	–	–	–
-0.7729	0.0996	0.6266	5.093 ± 0.084	5.077	3.084 ± 0.112	3.104	–	–
0.0322	0.9945	-0.0992	4.686 ± 0.077	4.683	3.045 ± 0.040	3.058	–	–
-0.5842	-0.0799	-0.8077	4.810 ± 0.194	4.785	–	–	–	–
0.1276	0.9916	-0.0222	4.699 ± 0.125	4.716	3.009 ± 0.025	3.051	2.782 ± 0.194	2.809
0.7249	-0.1195	0.6784	4.833 ± 0.115	4.852	3.151 ± 0.070	3.184	2.929 ± 0.192	2.868
0.6324	-0.1587	-0.7582	–	–	3.204 ± 0.092	3.184	2.811 ± 0.224	2.748

exp. – Experimentally measured values; cal. – values calculated inversely from refined elastic constants.

2H phase (Table 7) were evaluated using the optimization method (Section 2.3) considering all results in Table 6. The experimental error intervals for individual elastic

constants (Table 7) were estimated similarly as in the case of the austenite phase. The refined elastic constants (evaluated considering all data in Table 6) were used to

Table 7

Elastic constants of the orthorhombic 2H martensite phase in CuAlNi measured in this work and comparison with the constants available in the literature

Source	C_{11} (GPa)	C_{22} (GPa)	C_{33} (GPa)	C_{44} (GPa)	C_{55} (GPa)	C_{66} (GPa)	C_{23} (GPa)	C_{13} (GPa)	C_{12} (GPa)
This work	184.46 ± 1.12	151.45 ± 0.75	238.58 ± 1.87	66.39 ± 0.21	22.85 ± 0.18	60.55 ± 0.40	86.83 ± 1.05	70.09 ± 1.07	140.41 ± 0.77
[5]	189	141	205	54.9	19.7	62.6	124	45.5	115

calculate the acoustic wave velocities q_L , q_{T1} , q_{T2} . The obtained results (“cal.” in Table 6) can be compared with their experimental counterparts.

4. Discussion

4.1. Austenite elastic constants

As concerns the elastic constants of the CuAlNi austenite, numerous results were reported in the literature [8,11–13,16–18]. Due to the strong elastic anisotropy, the value of C' is very low compared to the constants C_{11} , C_{12} and C_{44} . Our results for C_{11} and C_{44} (Table 4) agree with the literature data. However, there are differences in the values of C_{12} , C' and A . Table 8 shows a summary of the literature data of C' we are aware of. Since C' varies with temperature (with $T - T_0$), results measured on different alloys can not be compared in a straightforward manner without taking into account chemical composition and heat treatments resulting in different M_s (T_0) temperatures of the martensitic transformation. The value of C' (9.14 ± 1.09 GPa) measured in this present work is larger than all earlier reported results, except that in [12] ($C' = 9.2$ GPa). The relatively high value of C' just above the M_s temperature results in the low elastic anisotropy factor ($A = 10.42 \pm 1.24$) found in the present work, and is among the lowest of the values reported in the literature ($A = 10$ – 13).

The standard pulse-echo method adopted by most of the authors (Table 8) is based on direct evaluation of

three independent elastic constants from pulse-echo measurements on prism shaped specimen of supposedly exact crystallographic orientation of the faces (1 1 0)–(1 1 0)–(0 0 1) using Eqs. (1) and (2). The “low-valued” quasi-shear velocity ((1 $\bar{1}$ 0) transverse waves along (1 1 0)) corresponding to the C' is very difficult to measure precisely by the pulse-echo ultrasonic method, since the corresponding echoes of slowly propagating transverse acoustic waves may be influenced or overlapped by faster waves refracted at the surfaces of the specimen. We believe that the large experimental error stemming from uncertainties in crystal orientations as well as from difficulties with the measurement of the constant C' (Eq. (3)) using the pulse-echo method could be the cause of the scatter in the values of the elastic constants available in the literature (Table 8).

We repeated carefully both the acoustic measurements and elastic constant refinement with the error analysis, but the results always approached the relatively high value of C' (Table 7). The experimental uncertainty is still relatively large ($\sim 12\%$), in spite of the fact that the present weighted optimization procedure suppresses the importance of acoustic modes difficult to measure experimentally as well as the uncertainty in determining the crystallographic orientation. If one takes into account the estimated confidence interval, the presently reported value is not so far from the literature values measured by the RUS method (7.56–8.4 GPa depending on temperature [11,13]) The resonant technique is more suitable for evaluation of the elastic constants C' with high precision, since C' corresponds to the easily measurable low

Table 8

Summary on the literature data concerning the C' elastic constant of the austenite phase in CuAlNi

Alloy composition	Refs.	M_s (K)	C'		$d \ln C' / dT$ ((1/K) 10^4)	Experimental method (–)
			At 295 K ($T - M_s$)	near M_s		
			(GPa)/(K)	(GPa)		
Cu _{2.742} Al _{1.105} Ni _{0.152}	[11]	260	7.34/(35)	7.22	4.36	Pulse-echo
Cu _{2.726} Al _{1.122} Ni _{0.152}	[11]	220	7.48/(75)	7.23	4.25	Pulse-echo
Cu–14wt.%Al–4.1wt.%Ni	[12]	249	9.41/(46)	9.20	3.20	Pulse-echo
Cu–14wt.%Al–4.1wt.%Ni	[17]	–	7.6–8.2 ^a /–	–	–	–
Cu–14.5wt.%Al–3.15wt.%Ni	[18]	–	8.5/–	–	–	–
Cu–27.96at.%Al–3.62at.%Ni	[11]	226	7.81/(69)	7.56	4.20	RUS
Cu–14.1wt.%Al–3.0wt.%Ni	[8]	–	7.05/–	–	–	–
Cu–14.3wt.%Al–4.1wt.%Ni	[13]	170	8.40/(125)	7.98	3.97 ± 0.04	RUS

RUS – resonant ultrasound spectroscopy.

^a Scatter in C' in dependence on quenching treatment affecting the M_s temperature of the alloy.

resonant frequencies. The decreasing trend of C' with decreasing temperature down to M_s was confirmed in both [11,13].

4.2. Martensite elastic constants

The development of the deformation techniques (Section 3.2) used to prepare the martensite parallelepiped single crystal variants for the ultrasonic measurement was essential for the successful evaluation of martensite elastic constants. Although it is outside the scope of this work to discuss in detail the deformation mechanisms of CuAlNi single crystals, the results of the compressive deformation treatments themselves deserve at least brief comment. Let us look first at the stress-induced martensitic transformation taking place during compression loads on austenite samples. The stress-induced bcc \rightarrow 2H martensite transformation takes place in the test denoted as AM-C in Fig. 3(a) (load axis orientation near $[1\ 1\ -2]_A$). Although there is no theoretical possibility for the existence of the habit plane between austenite and a single lattice correspondent variant (LCV) of the 2H phase, the transformation occurring during the plateau range of the σ - ϵ curve seems to proceed into the detwinned martensite variant. As viewed in an optical microscope attached to the testing machine, the deformation was localized into a single martensite band which nucleated suddenly and propagated through the sample until the end of the plateau. Lots of thin martensite bands were observed to appear temporarily prior to the nucleation event and near the moving macroscopic interface within both phases. The transformation was not reversible upon unloading. On the other hand, reversible pseudoelastic σ - ϵ response with much narrower stress hysteresis was recorded in the AM-A test (load axis orientation near $[3\ -4\ 0]$). This is because in this particular case, the monoclinic 18R phase with small hysteresis was induced, instead of the orthorhombic 2H martensite phase. This is well known to occur in compression tests on CuAlNi [1] when the load axis approaches the $[0\ 1\ 1]$ - $[\bar{1}\ 1\ 1]$ zone directions. No stress-induced transformation was observed in AM-B test (load axis orientation near $[8\ 5\ 7]$), since the transformation stress for both bcc \rightarrow 2H and bcc \rightarrow 18R transformations becomes very high when load axis orientation approaches the $[1\ 1\ 1]$ crystal direction [1]. The loading had to be interrupted at 250 MPa compressive stress because of the load cell limits. More information on the anisotropy of pseudoelastic deformation of CuAlNi single crystals in compression (evidence of orientation dependence of stresses, strains and Young's moduli) can be found in [1].

As regards the orientation dependence of σ - ϵ responses upon compression loading in the martensite

state, a variety of responses similar to that denoted as MM-AC in Fig. 3(a) (one or two stress plateaus of various stress level and length) were recorded in various experiments depending on load axis orientation and history. If it exists, the first low stress plateau (typically <5 MPa) on the two stage σ - ϵ curve corresponds to the $(1\ 0\ 1)\gamma'_1$ compound twinning, the second plateau (typically ~ 30 to 50 MPa) corresponds to Type I or Type II twinning depending on the orientation of the compression load axis. The stress-strain responses in the martensite phase thus depend first of all on the activated twinning mode in the 2H martensite phase. As far as we know, there exists only the data reported by Otani et al. [14] concerning the orientation dependence of twinning modes in CuAlNi 2H martensite single crystals. As they showed, the 2H crystals loaded in tension typically changed their orientation by twinning once or twice before ultimately being transformed into β'_1 18R martensite phase. The 2H \rightarrow 18R transformation does not commonly take place in compression since the 2H martensite phase provides similar or even larger compression strains along the load axis than the β'_1 18R martensite [1] for most of the crystal orientations. The twinning processes in the 2H martensite phase during compression deformation are currently being systematically studied and the results will be reported elsewhere.

Let us point out that good martensite parallelepiped single crystals could only be prepared thanks to the fact that frictional forces between grips and sample faces did not prevent the crystals undergoing the very large shape changes demonstrated in Fig. 4. Nevertheless, it still happened very often that two variants were induced in the sample and remained locked in some geometrical configuration at the end of deformation plateaus of σ - ϵ curves (Fig. 3). In this case, even if the σ - ϵ curve exhibited a compression strain correct for a particular martensite variant, the required agreement between the experimental and calculated sample shapes was not achieved. Such martensite samples were not used in pulse-echo measurements. The essential role of using the sample shape measurements instead of axial strain only for characterization of martensite variant single crystals is evident.

As concerns the values of elastic constants of the 2H martensite phase, we are aware solely of the frequently referenced results by Yasunaga et al. [5] (Table 7), who prepared martensite single crystal by cooling under stress from the austenite phase, cut one small oriented martensite single crystal and employed the RUS technique taking into account very low number of resonance frequencies. Since the authors [5] did not specify the orientation of the martensite coordinate system, we ordered their elastic constants in Table 7, so that they best match our values. Although the results are quite similar, there remain discrepancies to be resolved in future work.

4.3. Inheritance of special acoustic modes from austenite into martensite

Looking at the martensitic transformation as being due to the instability of the crystals with respect to strains in the crystal lattice, it is instructive to follow the variation of elastic constants of both phases with temperature or stress up to the stability point [3,6,13] as well as to evaluate discontinuous changes of elastic constants with the martensitic transformation [6]. An extensive recent review on temperature and stress variations of elastic constants for β -phase alloys can be found in [3]. The discontinuous changes of elastic constants with the martensitic transformation are focused upon in the present work. It is essential that the elastic constants of both austenite and 2H martensite phases in CuAlNi were evaluated on the same sample at the same temperature. In order to inspect the soft shear modes of a crystal structure, it became common in the literature [3] to compute the velocities of transverse acoustic waves from elastic constants and plot variation of the acoustic wave velocity with crystal directions in selected crystal planes or construct wave velocity surfaces in a form of spherical polar diagrams. This approach has been adopted in the present work and applied to both longitudinal and transverse acoustic waves with the aim of inspecting the inheritance of soft acoustic modes and elastic properties from the austenite to the martensite phase.

In order to compare the velocity surfaces corresponding to qL, qT1 (fast) and qT2 (slow) waves for austenite and martensite phases they were plotted in such a way that the lattice corresponding planes in both phases are aligned (Fig. 5(b)). The wave velocity surfaces are spherical polar diagram showing surfaces generated by vectors \mathbf{v}^A , \mathbf{v}^M expressed by

$$\mathbf{v}^A = v^A(\mathbf{n}^A)\mathbf{n}^A, \quad (11)$$

$$\mathbf{v}^M = v^M(\mathbf{n}^M)\mathbf{n}^A, \quad (12)$$

$$[\mathbf{n}^M]^T = \mathbf{S}\mathbf{P}_i[\mathbf{n}^A]^T, \quad (13)$$

where \mathbf{n}^A is a direction of wave propagating in austenite, \mathbf{n}^M the corresponding direction in martensite, $v^A(\mathbf{n}^A)$ and $v^M(\mathbf{n}^M)$ are wave velocities in given directions, the matrix $\mathbf{S} = \text{diag}(1/a; 1/b; 1/c)$ and \mathbf{P}_i is the transformation matrix for planes (Eq. (9), Table 5) and superscript T denotes transpose.

Since the martensitic transformation is mainly related to stability of shears, we are particularly interested in certain special points on the velocity surfaces of transverse acoustic waves. Due to the definition of qT1 as fast and qT2 as slow waves, the minima will always appear on the qT2 surface. Fig. 5(a) shows the part of the qT2 velocity surface of the austenite phase for the quadrant cut by planes $(0\ 0\ 1)_A$ and $(1\ 0\ 0)_A$. The highly sym-

metric surface displays two kinds of special points – the minima at $\mathbf{v}_{C'}$ (12 minima) and \mathbf{v}_{C_S} (24 saddle points) directions. The former corresponds to elastic constant C' representing the total minimum of shear stiffness in $[1\ 1\ 0]_A\{1\ -1\ 0\}_A$ shear systems in CuAlNi [2,3]. These low value shear modes significantly soften [3] with decreasing temperature towards M_s . The \mathbf{v}_{C_S} minima in planes $\{1\ 1\ 0\}_A$ were denoted C_S according to Nagasawa et al. [19]. They are saddle points on the velocity surface as become evident in the 3D view in Fig. 5(a). The velocity of transverse acoustic wave \mathbf{v}_{C_S} propagating in C_S directions characterized by angle Θ_S from $[1\ 0\ 0]_A$ direction in $(0\ 1\ 1)_A$ plane (Fig. 5(f)) is given by

$$\Theta_S = \sin^{-1} \sqrt{2(C_{11} + C_{12}) / (3C_{11} + 5C_{12} + 2C_{44})}, \quad (14a)$$

$$\rho v_{C_S}^2 = C_S = C' + 0.5(C_{44} - C')\sin^2 \Theta_S. \quad (14b)$$

Softening of the C_S mode has never been reported for CuAlNi as far as we know, but it was observed for other materials such as NiAl, NiTi [4,19]. When the martensitic transformation proceeds, the shears corresponding to C' and C_S are considered to play crucial role in the martensite formation of bcc solids according to Burgers scheme [4,19]. While the shears $[1\ 1\ 0]_A\{1\ -1\ 0\}_A$ (C') bring the $\{1\ -1\ 0\}_A$ planes into their close-packed formation within the martensite structure, the special mode shears $\langle 1\ -1\ -1 \rangle_A\{1\ -1\ 2\}_A$ (C_S) are considered to be responsible for the particular stacking structure within the martensite [19]. Therefore, we are interested in how the special points on the austenite velocity surfaces corresponding to C_{44} , C' and C_S (Fig. 5(a)) are inherited by the martensite phase after the phase transformation takes place.

The austenite velocity surface is compared with 1st variant velocity surface of the 2H martensite in Fig. 5(b). It is to be noted that austenite planes $(0\ -1\ 1)_A$ and $(0\ 1\ 1)_A$ become principal planes $(0\ 0\ 1)_M$ and $(1\ 0\ 0)_M$ in the 1st variant of the martensite phase and that formation of this 1st variant is favored by a compression stress applied along the $[1\ 0\ 0]_A$ crystal direction (Fig. 2(a)), for example. The martensite velocity surface (Fig. 5(b)) was inspected for the special points and the result of this search is summarized in Table 10, where wave velocities and unit vectors in the propagation and polarization directions corresponding to the special points are given. Local minima were found at \mathbf{v}_{M1} (two minima) and \mathbf{v}_{M2} (two minima) directions lying in the principal martensite planes $(0\ 0\ 1)_M$ and $(1\ 0\ 0)_M$, respectively. These local minima are associated with $\langle 1\ 0\ 0 \rangle_M(0\ 0\ 1)_M$ and $\langle 0\ 0\ 1 \rangle_M(1\ 0\ 0)_M$ shears corresponding to C_{55} elastic constants of the martensite phase. Total minimum was found in general martensite crystal direction \mathbf{v}_{M3} (eight equivalent minima) lying in a kind of “valley” on the martensite velocity surface (four equivalent valleys). There are four pairs of M3 minima

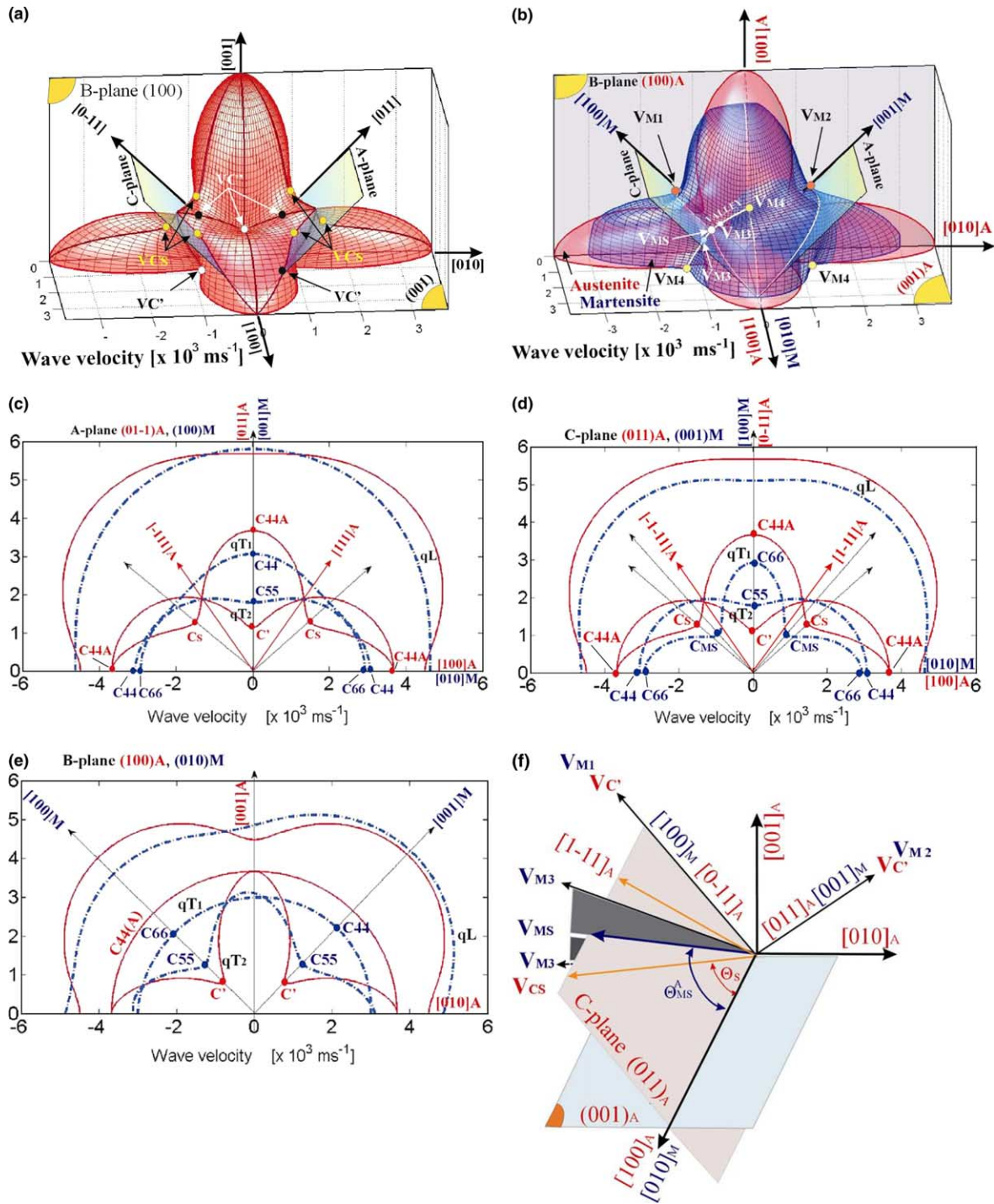


Fig. 5. Orientation dependences of velocities of ultrasonic waves (velocity surfaces) propagating in the austenite and 1st variant martensite phases. Part (a) shows one quadrant of spherical polar diagrams of the qT2 velocity surface of quasi-transverse waves propagating in the austenite. (b) Comparison of the qT2 velocity surfaces of austenite and the martensite using the lattice plane correspondence. Points v_C and v_{M3} correspond to crystal directions in the austenite (v_C) and martensite (v_{M3}) phases, in which the qT2 waves propagate with the slowest velocities. Surface sections of the velocity surfaces of all the three acoustic waves qL, qT1 and qT2 along crystal planes A – (0 1 -1)_A (c), B – (0 1 1)_A (d) and C – (1 0 0)_A (e) are shown for both austenite (solid lines) and martensite (dashed lines) phases. Points corresponding to special acoustic modes (see Tables 9 and 10) of both phases are denoted. The sketch in (f) shows the geometrical details concerning the martensite special mode v_{MS} .

(Figs. 5(f) and 6) centered around the v_{MS} direction in the (0 0 1)_M martensite basal plane (four equivalent v_{MS} directions). The points in the (0 0 1)_M basal plane

denoted v_{MS} (Fig. 5(b)) are thus in fact saddle points in the mentioned valleys (four equivalent saddle points).

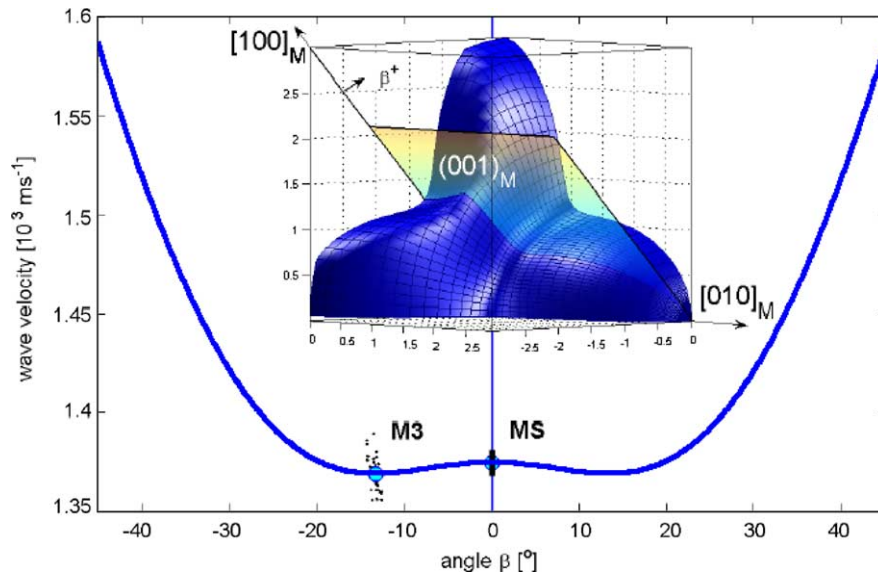


Fig. 6. Velocity profile of the “valley” on the 2H martensite qT2 velocity surface. Velocity minima found in sections along $(h\ 0\ l)_M$ planes (crystal planes in the $[0\ 1\ 0]_M$ zone) are plotted in dependence on angle β between the $(h\ 0\ l)_M$ plane and the basal $(0\ 0\ 1)_M$ plane. The cloud of points around the M3 point are the results of 50 calculations of the velocity surface from 2H elastic constants scattering randomly within the error intervals given in Table 7.

Let us now look more closely on the inheritance of the austenite soft modes into particular martensite variant. Inheritance of the soft modes into the 2H martensite phase in CuAlNi was mentioned by Yasunaga et al. [5] and some comments on CuZnAl alloy transforming into 18R monoclinic martensite can be found in [3,6]. However, as far as we know, the inheritance was never investigated in detail and not specifically for a transformation into a particular martensite variant selected by external stress, since the elastic constants for both phases in a single specimen at the same temperature were not available. The inheritance of the soft modes is more conveniently presented using sections through the velocity surfaces (Figs. 5(c)–(e)). One can straightforwardly read from these diagrams how the velocities of qL, qT1 and qT2 acoustic waves change along particular crystal directions with the martensitic transformation. Let us look first at the M1 and M2 local minima. They relate to the C_{55} elastic constant of orthorhombic lattice. Considering that both the propagation and polarization vectors in the martensite $(\langle 1\ 0\ 0 \rangle_M \langle 0\ 0\ 1 \rangle_M)$ and $(\langle 0\ 0\ 1 \rangle_M \langle 1\ 0\ 0 \rangle_M)$ exactly correspond (Table 10) to those representing the aus-

tenite C' mode $(\langle 0\ 1\ 1 \rangle_A \langle 0\ 1\ -1 \rangle_A)$ and $(\langle 0\ -1\ 1 \rangle_A \langle 0\ 1\ 1 \rangle_A)$ and both are pure modes (Table 9, Figs. 5(c)–(e)), it is obvious that the $C_{55} = 22.85$ GPa martensite constant was inherited from the $C' = 9.14$ GPa austenite constant. Recalling that variant 1 preferably forms under uniaxial compressive stress applied along $[0\ 1\ 0]_M$ direction or tensile stress along $[1\ 0\ 0]_M$ direction, we see that the C_{55} martensite soft shears were inherited from those austenite soft C' shears, the interaction of which with the applied stress was minimal when the martensite phase formed.

In order to understand where the global minima M3 on the martensite velocity surface come from, we have to look more closely at the earlier mentioned deep valley. The valley represents a major symmetry breaking change of the austenite velocity surface introduced by the martensitic transformation. Each valley contains the two global minima at v_{M3} directions and one saddle point at v_{MS} direction in the basal plane $(0\ 0\ 1)_M$. The corresponding elastic constants are $C_{M3} = 13.22$ GPa and $C_{MS} = 13.33$ GPa. Since these values are very close, we were suspicious whether the origin of the M3 minima

Table 9
Characteristics of special points on velocity surfaces of transverse acoustic waves propagating in austenite phase

Special point	Mode type	N_E	Velocity (10^3 m/s)	Propagation direction in austenite coordinates			Polarization direction in austenite coordinates		
C'	T	12	1.138	0.707	-0.707	0	0.707	0.7071	0
C_S	qT	24	1.980	0.755	-0.464	0.464	0.755	0.464	-0.464
C_{44}	T	-	3.674	[h k 0]			0	0	1

N_E denotes number of geometrically equivalent points from symmetry reasons; qT and T denote quasi-shear and shear modes, respectively.

Table 10

Characteristics of special points on velocity surfaces of transverse acoustic waves propagating in martensite phase

Special points in martensite	Mode type	N_E	Velocity (10^3 m/s)	Propagation direction in martensite coordinates			Polarization direction in martensite coordinates			Corresponding special points in austenite
M1(C_{55})	T	2	1.800	1	0	0	0	0	-1	C'
M2(C_{55})	T	2	1.800	0	0	1	1	0	0	C'
M3	qT	8	1.369	0.673	0.722	0.160	0.673	-0.722	0.160	–
MS(C_{MS})	qT	4	1.375	0.688	0.726	0	-0.688	0.726	0	C_S
M4	qT	8	1.603	0.494	0.703	0.513	-0.668	0.693	-0.272	C'
C_{44}	T	2	3.068	0	0	1	0	1	0	C_{44}
C_{44}	T	2	3.068	0	1	0	0	0	1	C_{44}
C_{66}	T	2	2.930	1	0	0	0	1	0	C_{44}
C_{66}	T	2	2.930	0	1	0	1	0	0	C_{44}

N_E denotes number of geometrically equivalent points from symmetry reasons; qT and T denote quasi-shear and shear modes, respectively.

could be just due to experimental errors and numerical procedures. A stability check (50 calculations) has been carried out by calculating the velocity surfaces from randomly chosen elastic constants within the range of their error intervals (Table 7). It was found that, surprisingly, not only the very existence of the M3 minimum, but also its location is stable in the range of the error intervals. This is documented in Fig. 6, where the values of the velocity minima found in sections along $(h\ 0\ l)_M$ planes (crystal planes in the $[0\ 1\ 0]_M$ zone) are plotted in dependence on angle β between the $(h\ 0\ l)_M$ plane and the basal $(0\ 0\ 1)_M$ plane. It is evident from the reported scatter in the location of M3 minima that the precision of its determination is good enough to distinguish it clearly from the saddle point MS, in spite of very small differences in velocities. Fig. 6 clearly documents the special character of the global velocity minima of the 2H martensite phase in the “valley” as two M3 minima connected through the MS saddle point in the basal $(0\ 0\ 1)_M$ plane. Since the MS point best characterizes the deep valley and hence the related martensite non-basal soft modes, we are particularly interested in its characteristics (Table 10).

Since the \mathbf{v}_{MS} direction lies in the symmetry plane of the martensite structure, it was possible to express analytically the velocity \mathbf{v}_{MS} and propagation direction Θ_{MS} of the transverse acoustic wave as a function of 2H elastic constants

$$\sin^2 \Theta_{MS}^{1,2} = \frac{-K_{10} \pm \sqrt{K_{10}^2 - 4K_9 K_{11}}}{2K_9}, \quad (15a)$$

$$\begin{aligned} \rho v_{MS}^2 &= C_{MS} \\ &= \min_{j=1,2} \left\{ \frac{1}{2} \left(K_1 + K_2 \sin^2 \Theta_{MS}^j \right. \right. \\ &\quad \left. \left. - \sqrt{K_6 \sin^4 \Theta_{MS}^j + K_7 \sin^2 \Theta_{MS}^j + K_8} \right) \right\}, \quad (15b) \end{aligned}$$

where $K_1 = C_{66} + C_{22}$, $K_2 = C_{11} - C_{22}$, $K_3 = (C_{11} - C_{66})(C_{66} - C_{22}) + (C_{12} + C_{66})^2$, $K_4 = C_{66}K_2 - K_3$, $K_5 = C_{66}C_{22}$, $K_6 = K_2^2 - 4K_3$, $K_7 = 2K_1K_2 - 4K_4$, $K_8 = K_1^2 - 4K_5$,

$K_9 = K_3K_6$, $K_{10} = K_3K_7$, $K_{11} = K_1K_2K_4 - K_2^2K_5 - K_4^2$. The angle Θ_{MS} characterizes the propagation direction by an angle between \mathbf{v}_{MS} and $[0\ 1\ 0]_M$ in the $(0\ 0\ 1)_M$ plane (Fig. 5(f)) in an analogy to the Θ_S (Eq. (14a)) characterizing the C_S special mode of the austenite phase. Let us call the acoustic mode corresponding to the \mathbf{v}_{MS} direction a martensite special mode C_{MS} (Eq. (15b)). The obtained value of angle $\Theta_{MS} = 43.5^\circ$ may be recalculated into the angle $\Theta_{MS}^A = 47.8^\circ$ between the propagation direction and the austenite direction $[1\ 0\ 0]_A$ using the correspondence (13) of the crystallographical planes. Note that angles Θ_S and Θ_{MS}^A (Fig. 5(f)) are different and it may be shown that polarization vectors of both modes are not exactly aligned (inherited). In spite of that, the martensite special mode C_{MS} and austenite special mode C_S seem to be clearly related. The wave velocity corresponding to C_{MS} mode is however smaller compared to that corresponding to the C_S mode (Table 9, Fig. 5(d)); comparing the elastic constants, $C_S = 27.67$ GPa $>$ $C_{MS} = 13.33$ GPa. This is surprising since one would expect stiffening of the soft modes with the martensitic transformation as it occurs for the $C' \rightarrow C_{55}$ inheritance (Table 10, Figs. 5(d) and (e)). In fact, only four austenite C_S modes lying in the $(0\ 1\ 1)_A$ plane (the $\{0\ 1\ 1\}_A$ which becomes $(0\ 0\ 1)_M$ basal martensite plane) soften during the discontinuous change of the elastic properties with the martensitic transformation. The remaining eight austenite C_S modes harden. Finally, it shall be mentioned that the direction of the \mathbf{v}_{M4} velocity lying also in the valley (Fig. 5(b)), does not in fact mark an extremum or otherwise special point on the martensite velocity surface. The M4 points were included in Fig. 5(b), since they mark the martensite modes (apparent minima in sections along $(0\ 1\ 0)_A$ planes) inherited from the remaining eight soft C' modes of the austenite phase not related to the M1 and M2 minima. The wave velocities corresponding to \mathbf{v}_{M4} directions are larger than that of the C' mode of the austenite but smaller than that corresponding to C_{55} mode of the martensite (minima M1, M2). The valley characterized by the martensite special mode C_{MS} is thus an essential feature of the 2H martensite velocity surface

which is likely to be important for the stability of 2H structure. The results of González-Comas et al. [6], who studied temperature dependence of elastic properties of similar 18R martensite in CuZnAl, seem to suggest that the velocity surface of the 18R phase is somehow different (the special point MS does not exist) and that some of the 18R elastic constants vary significantly with the temperature approaching A_f . This remains to be further investigated in future work.

Figs. 5(c)–(e) also provide information on the fast qT1 transverse acoustic waves not considered in Figs. 5(a) and (b). The maxima on the qT1 velocity surface corresponding to C_{44} elastic constant of the austenite (C44A in Figs. 5(c)–(e)) are inherited by the martensite phase as either C_{44} and C_{66} elastic constants. The wave velocities in the martensite phase corresponding to C_{44} and C_{66} modes are rather similar (Table 9) and smaller compared with the velocity corresponding to the parent C_{44} austenite mode. The velocity of qT1 fast acoustic wave thus exhibits softening almost everywhere except in the direction close to $[1\ 1\ 1]_A$. If we take the ratio of maximum and minimum characteristic shears A^{ort} as a criterion for elastic anisotropy of the orthorhombic 2H structure,

$$A^{ort} = \frac{C_{44}}{C_{MS}} \quad (16)$$

We find ($A^{ort} = 3.49$) that the 2H martensite is less elastically anisotropic than the bcc austenite. Since geometrical details of the martensite acoustic modes (particularly C_{MS}) depend strongly on the actual values of the martensite elastic constants, we would like to obtain first an independent confirmation of the martensite elastic constants by the RUS method (this work is currently in progress) before going further with the interpretation of the presented results.

We should also briefly comment on the inheritance of the velocity surface corresponding to the longitudinal acoustic waves qL. The qL surface primarily brings information on the C_{11} elastic constant (Eq. (1a)). However, since the velocity in general crystal directions of anisotropic crystals depends also on other elastic constants (e.g., Eq. (2a) holds for the velocity in $[0\ 1\ 1]_A$ direction of the austenite phase), the qL velocity is orientation dependent. The shape of the qL surface of the austenite is in the first approximation inherited by the product martensite phase (Figs. 5(c)–(e)). It seems that softening (in a sense that velocity is lower in the martensite phase) prevails for most of the crystal directions, though there are some specific directions (e.g. $\langle 1\ 0\ 1 \rangle_M$ and $\langle -1\ 0\ 1 \rangle_M$ (Fig. 5(e))), where the qL velocity significantly increases. The qL surface is relatively uninteresting for the lattice stability of martensitically transforming bcc alloys, but important for the anisotropy of elastic properties of both phases and change of elastic properties with the transformation (Section 4.4).

The changes of the velocity of longitudinal ultrasonic waves with the stress-induced martensitic transformation were measured experimentally in our previous work dealing with CuAlNi cubes [2]. Fig. 7, which has been redrawn from data reported in [2], shows a relative change of the velocity of qL-wave propagating in $[0\ -1\ 1]_A$ direction perpendicularly to the compression load axis $[1\ 0\ 0]_A$ during a pseudoelastic test on CuAlNi single crystal cube ($M_s = 193\text{ K}$). In the elastic range, the velocity at first slightly increases with increasing applied stress (this corresponds to positive third order elastic constant [2]). When the stress-induced transformation starts at $\sigma = 350\text{ MPa}$, however, the wave velocity drastically decreases (8%). Reverse stepwise change of the velocity is observed during the reverse transformation

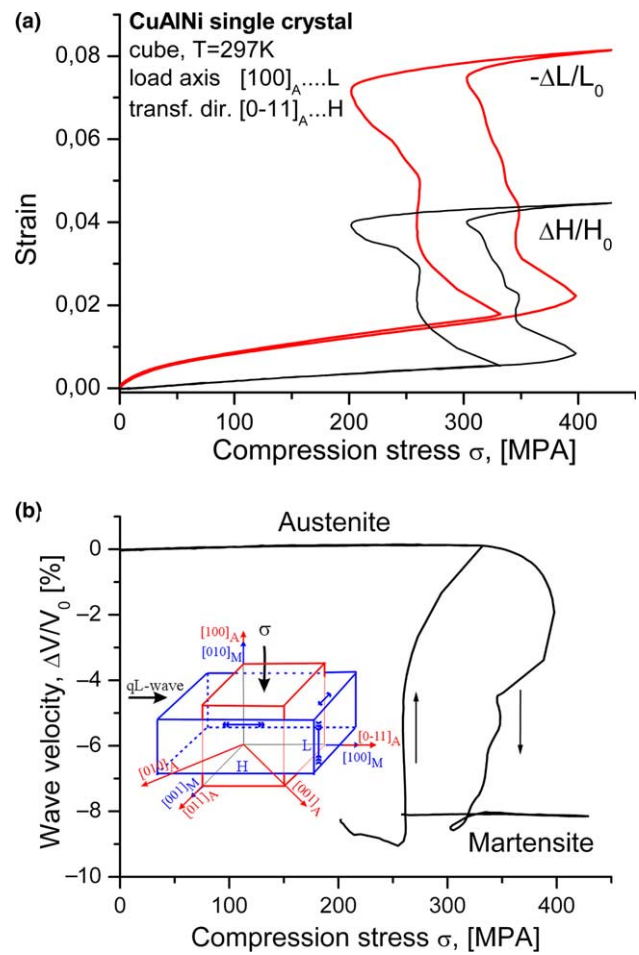


Fig. 7. In situ ultrasonic measurement on CuAlNi single crystal cube ($M_s = 193\text{ K}$, $a = 10\text{ mm}$, faces $(0\ 1\ 1)_A$, $(0\ -1\ 1)_A$, $(1\ 0\ 0)_A$), redrawn from [2]. The cube was deformed pseudoelastically at $T = 297\text{ K}$ ($M_s + 104\text{ K}$) in compression (a) along the $[1\ 0\ 0]_A$ crystal direction ($\Delta L < 0$). The velocity of the longitudinal acoustic wave qL propagating along perpendicular $[0\ -1\ 1]_A$ crystal direction was measured simultaneously with the transverse dimensional change ($\Delta H > 0$). (a) The strains are plotted as a function of the applied stress. (b) The relative velocity change $\Delta V/V_0$ was normalized with respect to the transverse dimensional change $\Delta H > 0$. The cube changes into prism with the stress-induced transformation upon loading (inset in (b)).

upon unloading (at lower stresses due to the hysteresis). When the transformation is finished, the original values of strain and acoustic velocity are perfectly restored at ~ 300 MPa stress level and decrease upon further unloading down to zero stress. Notice the excellent reproducibility of the measured velocity out of the transformation range. When the qL velocity was measured in different crystal directions – i.e., along the second perpendicular direction $[0\ 1\ 1]_A$ or along the load axis $[1\ 0\ 0]_A$ (different experiment set up with ultrasonic sensors mounted inside the compression grips), a slight increase in the qL velocity upon forward loading was recorded in agreement with the calculated qL surfaces in Fig. 5(c)–(e).

These results provide direct experimental evidence that elastic constants of SMA single crystals change significantly with the stress-induced martensitic transformation and that these changes can be measured by ultrasound. The ultrasound would also detect thermally induced transformations and, due to elastic anisotropy, even twinning processes during martensite deformation. In situ ultrasonic measurements of acoustic wave propagation can be equally well applied to polycrystalline SMA samples transforming in thermomechanical cycles. Experiments on NiTi bars and wires [20,21] show large effects and very good reproducibility of acoustic wave velocities and attenuation measured in situ during thermomechanical cycles. The interpretation in terms of elastic property changes, however, is not as straightforward. Nevertheless, an idea to use ultrasound for non-destructive in situ studies of martensitic transformations in SMAs, similarly as e.g., electric resistivity, is currently seriously investigated. The combined electrical resistivity and ultrasonic in situ experimental method proposed in [21] can be utilized to distinguish various deformation/transformation processes in activated NiTi wires.

4.4. Elastic property changes with the austenite to martensite transition

Although some qualitative conclusions on the change of elastic properties with martensitic transformation can be deduced already from the orientation dependence of the acoustic wave velocities in Fig. 5, if we want to discuss the change of the elastic properties and anisotropy quantitatively [22], it is necessary to refer directly to the orientation dependence of some elastic properties. Since Young's modulus E is of wide interest, its variation with crystal direction was calculated from the measured elastic constants of both austenite and martensite phases from its definition [23,24] (Eqs. (17)–(19)). The compliance tensor S_{ijkl} is reciprocally related to the stiffness tensor C_{klmn} , i.e.,

$$S_{ijkl}C_{klmn} = \delta_{im}\delta_{jn}. \quad (17)$$

The component S_{1111} in a given direction \mathbf{d} is calculated for an arbitrary rotation (direction cosines a_{ij}) of the compliance tensor S_{ijkl}

$$S'_{1111} = a_{1m}a_{1n}a_{1p}a_{1q}S_{mnpq} \quad (18)$$

and Young's modulus $E(\mathbf{d})$ in the direction \mathbf{d} is calculated as

$$E(\mathbf{d}) = 1/S'_{1111}. \quad (19)$$

This procedure is applicable for general anisotropic solids and hence for both the austenite and martensite phases. Alternatively, Young's modulus in a given crystal direction $[h\ k\ l]$ for the cubic austenite phase can also be conveniently calculated directly from the elastic constants C_{ij} [23]

$$\frac{1}{E_{hkl}} = \frac{C_{11} + C_{12}}{(C_{11} - C_{12})(C_{11} + 2C_{12})} - 2 \frac{h^2k^2 + h^2l^2 + k^2l^2}{(h^2 + k^2 + l^2)^2} \left(\frac{1}{C_{11} - C_{12}} - \frac{1}{2C_{44}} \right). \quad (20)$$

The results are again presented using two interpenetrating spherical polar diagrams (Fig. 8) showing Young's moduli surfaces for austenite and 1st variant of the martensite phase (Fig. 2(a)). Similarly as in the case of wave surface comparison (Fig. 5), the Young's moduli surfaces in Fig. 8(a) are plotted for directions normal to the austenite lattice planes and lattice correspondent martensite planes (13). Only half of the surface is shown in Fig. 8(a) since the front plane is the mirror symmetry plane.

When analyzing the Young's moduli changes with phase transformation using Fig. 8, one immediately notices the large anisotropy of Young's modulus in both phases. In spite of the discontinuous change in elastic constants, the anisotropy of austenite is partially inherited by the martensite. The anisotropy of Young's moduli of the 2H martensite is characterized by three mutually orthogonal mirror planes (principal martensite planes A–C in Fig. 8(a)) of the orthorhombic elastic symmetry. The austenite Young's modulus surface has a complex shape with spikes of large moduli pointing along cube diagonals as common for bcc solids with large positive elastic anisotropy factor A [22,24]. Three sections of the Young's moduli surfaces along planes A–C are shown in Figs. 8(b) and (c) to present quantitative information on the change of the Young's modulus with the transformation. The austenite crystal was elastically hardest particularly along four cube diagonals $\langle 1\ 1\ 1 \rangle_A$ and softest along the three $\langle 0\ 0\ 1 \rangle_A$ directions. The 2H martensite in contrast becomes hardest in the $[0\ 0\ 1]_M$ martensite crystal direction but very soft in the $[1\ 0\ 0]_M$ (Figs. 8(b)–(d)). Note that both the $[0\ 0\ 1]_M$ and $[1\ 0\ 0]_M$ directions are lattice correspondent to the face diagonal $\langle 0\ 1\ 1 \rangle_A$ directions in the austenite phase. This represents the major symmetry breaking change in the anisotropy of Young's modulus with the transformation. As regards the minima, the

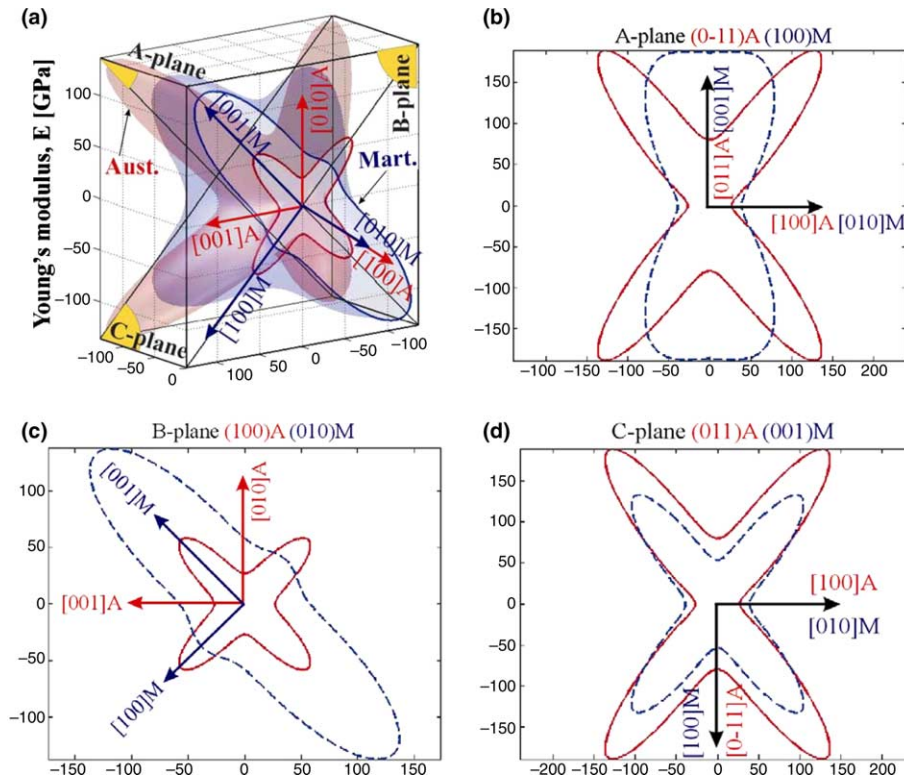


Fig. 8. Orientation dependence of Young's moduli of phases in CuAlNi single crystal calculated from elastic constants: (a) two interpenetrating spherical polar diagrams (half space) with Young's moduli surfaces of the austenite (solid line) and variant 1 of the 2H martensite (dotted line), (b–d) sections along three basic martensite planes, A – $(0\ -1\ 1)_A$ (b), B – $(1\ 0\ 0)_A$ (c), C – $(0\ 1\ 1)_A$ (d).

Young's modulus increases along all three $\langle 0\ 0\ 1 \rangle_A$ directions with the transformation, but since the increase is smallest along the $[0\ 1\ 0]_M$ direction, the martensite crystal becomes softest there (global minimum of the Young's modulus in the martensite). If we take the difference between minimal and maximal Young's moduli as an alternative qualitative criterion for the elastic anisotropy, we find the 2H martensite is less elastically anisotropic compared to the austenite phase. The anisotropy of the Young's modulus surface of the austenite phase is dominated by the soft C' shear modes. It appears that the anisotropy of the Young's modulus of the 2H martensite phase is partially inherited from the austenite phase ($C' \rightarrow C_{55}$) but modified particularly as a consequence of the soft non-basal shears corresponding to the deep valley on the qT2 velocity surface ($C_S \rightarrow C_{MS}$) discussed in Section 4.3.

Let us discuss briefly potential changes of the Young's modulus of the crystal with the stress-induced martensitic transformation. From a practical perspective, one is mainly interested in the change of Young's modulus along the direction of the load axis. Hence in doing that we have to at first check which martensite variant becomes induced by the applied stress. Let us consider the particular case of the pseudoelastic test shown in Fig. 7. In this case, the austenite cube sample with faces $(1\ 0\ 0)_A$, $(0\ 1\ -1)_A$, $(0\ 1\ 1)_A$ is compressed along the $[1\ 0\ 0]_A$ direction. Two

lattice correspondent martensite variants can be stress induced (1st and 2nd in Table 5) because they are equally preferred by the applied compression stress (the 1st and 2nd variants provide largest strain). If the variant 1 for which Figs. 8 and 4(a) apply is induced, the Young's modulus increases in the $[1\ 0\ 0]_A$ direction ($[0\ 1\ 0]_M$ direction in the martensite phase, contraction 8.46%), decreases in $[0\ 1\ -1]_A$ direction ($[1\ 0\ 0]_M$, dilatation 6.37%) and strongly increases in $[0\ 1\ 1]_A$ direction ($[0\ 0\ 1]_M$, dilatation 2.37%). In this very special geometrical case, the austenite cube changes after the transformation into the martensite prism as suggested in the inset in Fig. 7(b). The increase of the Young's modulus along the load axis with the transformation was found in the present case. However, this does not have to be always the case. Note that variant 1 will be also induced in the case where the same cube is "pulled" in tension along the $[0\ 1\ -1]_A$ direction. In this case, Young's modulus of the sample is predicted (Fig. 8(c)) to decrease with the stress-induced transformation into the 2H martensite phase. In fact, due to the orientation dependence of Young's moduli of both phases and selection of martensite variant by the applied stress, the change of Young's modulus of the sample with the transformation depends on load axis direction and sense of loading as calculated and shown in Fig. 9. While in compression, an increase in Young's modulus is observed for most of the load axis orientations except the corner near

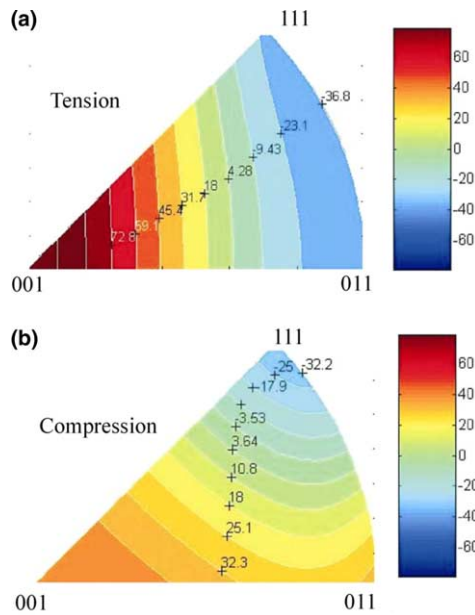


Fig. 9. Orientation dependence of the relative change of the Young's modulus with stress-induced bcc-2H martensitic transformation ($100 \times (E_M - E_A)/E_A$) is plotted over basic stereographic unit) upon uniaxial loading in tension and compression.

$\langle 111 \rangle_A$ directions, in tension, the Young's modulus decreases for wide range of load axis orientations near the $\langle 111 \rangle_A - (011)_A - \langle 111 \rangle_A$ zone and increases elsewhere. The decrease in Young's modulus with the phase transformation might have consequences on the stability of macroscopic deformation (localized vs. quasi-homogeneous deformation behavior) in pseudoelastic tests on CuAlNi single crystals.

It should be pointed out that the orientation dependence of Young's modulus does not fully characterize the peculiar elastic properties of the 2H martensite phase. In a similar fashion, one can investigate the orientation dependence of shear moduli or Poisson ratio in both phases and look at the inheritance of such elastic properties. For example, when the orientation dependence of Poisson ratio ν_{mn} is calculated from the elastic constants of the austenite, large negative values are obtained for some geometrical configuration of \mathbf{n} and \mathbf{m} vectors. The negative value of ν_{mn} means that CuAlNi crystal pulled in a direction \mathbf{n} extends in perpendicular direction \mathbf{m} . This property called auxeticity is rather common among strongly elastically anisotropic bcc solids. This auxeticity of the austenite phase is partially inherited into the orthorhombic 2H martensite as noticed also by Rovatti [25] who investigated theoretically the elastic properties of 2H crystal based on Yasunaga et al.'s constants [8].

Let us finally briefly comment on the macroscopic elastic property changes of SMA polycrystals transforming in thermomechanical loads. They can be measured experimentally by ultrasonic or mechanical means. The changes

of the elastic properties of NiTi with the transformation were evaluated by ultrasound [20]. These results, although rather difficult to properly interpret, are interesting from the point of view of mechanics modelling and engineering applications of SMAs. The macroscopic elastic properties of polycrystalline SMAs (e.g., Young's modulus of NiTi wire [21]) obviously depend very much on the crystallographic texture of the parent austenite phase. Particularly, the Young's modulus of a polycrystalline specimen depends on the load axis direction with respect to the texture. The question is how this macroscopic elastic anisotropy of the polycrystal is inherited by the martensite phase. This is a problem of the texture transformation accompanying martensitic transformation in SMAs. The texture which appears in the stress-induced martensite phase reflects partially the parent austenite texture. However, it is, in addition, strongly modified by the martensite variant selection under stress (as was investigated experimentally, e.g., for B19' martensite in NiTi [26]). The Young's modulus of the SMA polycrystal in fully deformed martensite state thus depends on the deformation history (on the previously applied stress state). In particular, since very different martensite textures typically appear in SMA polycrystals deformed in tension and compression [26], Young's modulus of deformed SMAs is expected to be different after deformation in tension and compression. In the particular case of CuAlNi polycrystals transforming to 2H phase, larger Young's modulus would be expected after compression than after tension, since the increase of the Young's modulus prevails for most of the crystal orientations in compression but not in tension (Fig. 9).

In view of the above discussion, the question of whether the martensite is softer or harder than the austenite raised frequently in the SMA modeling studies seems to have in fact little practical meaning. The martensite single crystal is elastically softer or harder than the austenite crystal depending on the direction we speak about. This is a consequence of the discontinuous change in elastic properties with the transformation, elastic anisotropy and lattice correspondence of both phases. The question whether the martensite polycrystal is elastically softer or harder than the austenite polycrystal is difficult but meaningful. Fig. 8(a) does not suggest any simple conclusion on the polycrystal Young's moduli change with the $\text{bcc} \rightarrow 2\text{H}$ transformation, except the obvious qualitative comment that the texture in parent austenite state and potential martensite variant selection during transformation would have a strong influence. Discussion of the polycrystal moduli is hence beyond the scope of this work. We can only remark that, in a deformed state, the Young's modulus of SMA polycrystals might depend on the deformation history, sense of load etc. and may be curiously different after tension and compression deformation due to the different selection of martensite variants by the tension and compression stress [26].

5. Summary and conclusions

Single crystals of CuAlNi alloy existing at room temperature either in austenite or martensite state were grown and cut into the cube shape ($a \sim 5.6$ mm) in austenite state. Taking advantage of the easy deformation twinning in the martensite state, multiple parallelepiped shaped samples were prepared by a compression deformation method. Ultrasonic pulse-echo measurements of the velocities of acoustic wave propagation were carried out on the austenite cubes as well as on the martensite parallelepiped shaped samples.

Elastic constants of cubic austenite and orthorhombic 2H martensite phases were evaluated using a newly developed optimization method which is based on inversion of ultrasound wave velocities measured in redundant number of general crystal directions. This method allows the minimization of uncertainties in evaluated elastic constants stemming from the experimental error in exact determination of the crystal orientation. It is believed that the optimization approach is more precise and less laborious particularly for low symmetry materials such as the orthorhombic 2H martensite phase in CuAlNi.

Taking advantage of the fact that the elastic constants of the austenite and 2H martensite phase were evaluated on the same material, soft acoustic modes and elastic properties of both phases were compared taking into account the lattice correspondence. The following conclusions were drawn: (i) The elastic properties change significantly with the martensitic transformation. (ii) The elastic properties of the austenite phase including the soft acoustic modes are only partially inherited by the martensite phase. (iii) Two soft acoustic modes of 2H martensite phase were identified $-(1\ 0\ 0)_M$, $(0\ 0\ 1)_M$ and $\langle 0\ 0\ 1 \rangle_M$ corresponding to C_{55} martensite elastic constant and soft non-basal shears corresponding to martensite special mode described by Eqs. (15a) and (15b). (iv) The 2H martensite crystal is less elastically anisotropic than the austenite. (v) Whether the martensite crystal is softer or harder than the austenite crystal depends on the crystal direction considered. This is a consequence of the discontinuous change in elastic properties with the transformation, elastic anisotropy and lattice correspondence of both phases.

Acknowledgements

Support of the Marie-Curie RTN Multimater (Contract No. MRTN-CT-2004-505226) is gratefully acknowledged. The work has been further supported by Czech Grant Agency under the project no. 106/03/1073, the

Grant Agency of Academy of Sciences A1048107, the project of the Institute of Thermomechanics ASCR No. AV0Z 20760514 and project MAT2004-1291 (CICyT, Spain).

References

- [1] Novák V, Šittner P, Vokoun D, Zárubová N. *Mater Sci Eng A* 1999;273:280.
- [2] Landa M, Novák V, Sedlák P, Šittner P. *Ultrasonics* 2004;42:519.
- [3] Planes A, Mañosa LI. *Solid State Phys* 2001;55:159.
- [4] Nakanishi N. *Prog Mater Sci* 1979;24:143.
- [5] Yasunaga M, Funatsu Y, Koijima S, Otsuka K, Suzuki T. *Scripta Metall* 1983;17:1091.
- [6] González-Comas A, Mañosa LI, Planes A, Lovey FC, Pelegrina JL, Guénin G. *Phys Rev B* 1997;56:5200.
- [7] Rodríguez PL, Lovey FC, Guénin G, Pelegrina JL, Sade M, Morin M. *Acta Metall* 1993;41:3307.
- [8] Yasunaga M, Funatsu Y, Koijima S, Otsuka K, Suzuki T. *J Phys (Paris)* 1982;3(Suppl.):603 [Cited as [82Y1] in Landolt HH. R. Börnstein NewSeries III/29a. Berlin: Springer-Verlag; 1992.].
- [9] Papadakis EP, Lerch TP. Pulse superposition, pulse-echo overlap and related techniques. In: Levy M, Bass HE, Stern RR, editors. *Handbook of elastic properties of solids, liquids and gases*, vol. I–IV. New York: Academic Press; 2001.
- [10] Auld BA. *Acoustic fields and waves in solids*, vol. 1. New York: John Wiley; 1973.
- [11] Mañosa LI, Jurado M, Planes A, Zarestky J, Lograsso T, Stassis C. *Phys Rev B* 1994;49:9969.
- [12] Hausch G, Török E. *J de Phys, Colloque C5* 1981;42:1031.
- [13] Landa M, Novák V, Sedlák P, Mañosa LI, Šittner P. *Mater Sci Forum* 2005;482:351.
- [14] Otani N, Funatsu Y, Ichinose S, Miyazaki S, Otsuka K. *Scripta Metall* 1983;17:745.
- [15] Otsuka K, Wayman CM, Nakai K, Sakamoto H, Shimizu K. *Acta Metall* 1976;24:207.
- [16] Recarte V, Pérez-Landazábal JI, Nó ML, San Juan J. *Mater Sci Eng A* 2004;370:488.
- [17] Suesawa M, Sumino K. *Scr Metall* 1976;10:789 [Cited as [76S11] in Landolt HH. R. Börnstein NewSeries III/29a. Berlin: Springer-Verlag; 1992.].
- [18] Zhailobaev KK, Serebryakov VG, Estrin EI. *Metallfizika* 1987;9:289 [Cited as [87Z3] in Landolt HH. R. Börnstein NewSeries III/29a. Berlin: Springer-Verlag; 1992.].
- [19] Nagasawa A, Nakanishi N, Enami K. *Philos Mag A* 1981;43:1345.
- [20] Šittner P, Landa M, Lukáš P, Novák V. *Mech Mater*, in press.
- [21] Šittner P, Landa M, Sedlák P, Lukáš P, Novák V. In: *Proceedings of SMST 2004*, Baden Baden, Germany, in press.
- [22] Ledbetter HM, Moment RL. *Acta Metall* 1976;24:891.
- [23] Nye JF. *Physical properties of crystals*. Oxford Scientific Publishers; 1957.
- [24] Cazzani A, Rovati M. *Int J Solids Struct* 2003;43:1713.
- [25] Rovati M. *Scripta Mater* 2003;48:235; *Scripta Mater* 2004;51:1087.
- [26] Šittner P, Neov D, Lukas P, Toebbens DM. *J Neutron Res* 2004;12:115.